Aerosol lidar intercomparison in the framework of the EARLINET project. 2. Aerosol backscatter algorithms

Christine Böckmann, Ulla Wandinger, Albert Ansmann, Jens Bösenberg, Vassilis Amiridis, Antonella Boselli, Arnaud Delaval, Ferdinando De Tomasi, Max Frioud, Ivan Videnov Grigorov, Arne Hågård, Matej Horvat, Marco Iarlori, Leonce Komguem, Stephan Kreipl, Gilles Larchevêque, Volker Matthias, Alexandros Papayannis, Gelsomina Pappalardo, Francesc Rocadenbosch, Jose António Rodrigues, Johannes Schneider, Valery Shcherbakov, and Matthias Wiegner

An intercomparison of aerosol backscatter lidar algorithms was performed in 2001 within the framework of the European Aerosol Research Lidar Network to Establish an Aerosol Climatology (EARLINET). The objective of this research was to test the correctness of the algorithms and the influence of the lidar ratio used by the various lidar teams involved in the EARLINET for calculation of backscatter-coefficient profiles from the lidar signals. The exercise consisted of processing synthetic lidar signals of various degrees of difficulty. One of these profiles contained height-dependent lidar ratios to test the vertical influence of those profiles on the various retrieval algorithms. Furthermore, a realistic incomplete overlap of laser beam and receiver field of view was introduced to remind the teams to take great care in the nearest range to the lidar. The intercomparison was performed in three stages with increasing knowledge on the input parameters. First, only the lidar signals were distributed; this is the most realistic stage. Afterward the lidar ratio profiles and the reference values at calibration height were

When this research was performed, C. Böckmann (bockmann@rz.uni-potsdam.de) was with the Institute of Mathematics, University of Potsdam Am Neuen Palais 10, 14469 Potsdam, Germany; U. Wandinger and A. Ansmann were with the Institute for Tropospheric Research, Permoserstrasse 15, 04303 Leipzig, Germany; J. Bösenberg was with the Max-Planck-Institut für Meteorologie, Bundesstrasse 55, 20146 Hamburg, Germany; V. Amiridis was with the Laboratory of Atmospheric Physics, Aristotle University of Thessaloniki, Box 149, 54124 Thessaloniki, Greece; A. Boselli was with the Istituto Nazionale per la Fisica della Materia, Complesso Universitario di Monte S. Angelo, via Cintia, 80126 Naples, Italy; A. Delaval was with the Institute Pierre Simone Laplace, Laboratoire de la Météorologie Dynamique, 91128 Palaiseau Cedex, France; F. De Tomasi was with the Istituto Nazionale per la Fisica della Materia, Dipartimento di Fisica, Universitá di Lecce, via Arnesano, 73100 Lecce, Italy; M. Frioud was with the Observatoire de Neuchâtel, Rue de l'Observatoire 58, 2000 Neuchâtel, Switzerland; I. V. Grigorov was with the Institute of Electronics, Bulgarian Academy of Sciences, Boulevard Tzarigradsko Chaussee 72, 1784 Sofia, Bulgaria; A. Hågård was with the Division of Sensor Technology, Swedish Defence Research Agency, P.O. Box 1165, 58111 Linköping, Sweden; M. Horvat was with the Laboratory for Astroparticle Physics, Nova Gorica Polytechnic, Vipavska 13, 5001 Nova Gorica, Slovenia; M. Iarlori was with the Departimento di Fisica, Universitá degli Studi—L'Aquila, Via Vetoio Localita Coppito, 67010 L'Aquila, Italy; L. Komguem was with the Department of Physics, University of Wales, Aberystwyth Ceredigion SY23 3BZ, United Kingdom; S. Kreipl was with the Institut für Meteorologie und Klimaforschung, Forschungszentrum Karlsruhe, Kreuzeckbahnstrasse 19, 82467 Garmisch-Partenkirchen, Germany; G. Larchevêque was with the Laboratoire de Pollution de l'Air et du Sol, École Polytechnique Fédérale de Lausanne, 1015 Lausanne, Switzerland; V. Matthias was with the Max-Planck-Institut für Meteorologie, Bundesstrasse 55, 20146 Hamburg, Germany; A. Papayannis was with the Department of Physics, National Technical University of Athens, Heroon Polytechniou 9, 15780 Zografou, Greece; G. Pappalardo was with the Istituto di Metodologie per l'Analisi Ambientale, Consiglio Nazionale delle Ricerche, Contrada S. Loja, 85050 Tito Scalo (Potenza), Italy; F. Rocadenbosch was with the Department of Signal Theory and Communication, Universitat Politècnica de Catalunya, Jordi Girona 1-3, Edifici D4-016, 08034 Barcelona, Spain; J. A. Rodrigues was with the Centro de Física de Plasmas, Instituto Superior Técnico, Avenida Rovisco Pais, 1049-001 Lisbon, Portugal; J. Schneider was with the Leibniz-Institut für Atmosphärenphysik Schlossstrasse 6, 18225 Kühlungsborn, Germany; V. Shcherbakov was with the Institute of Physics, National Academy of Sciences of Belarus, 68 F. Scarina Avenue, 220072 Minsk, Belarus, and M. Wiegner was with the Meteorologisches Institut, Ludwig-Maximilians-Universität München, Theresienstrasse 37, 80333 Munich, Germany. V. Matthias is now with the Institute for Coastal Research, GKSS Research Center, Max-Planck-Strasse 1, 21502 Geesthacht, Germany. J. Schneider is now with the Max-Planck-Institut für Chemie, 55020 Mainz, Germany.

provided. The unknown height-dependent lidar ratio had the largest influence on the retrieval, whereas the unknown reference value was of minor importance. These results show the necessity of making additional independent measurements, which can provide us with a suitable approximation of the lidar ratio. The final stage proves in general, that the data evaluation schemes of the different groups of lidar systems work well. © 2004 Optical Society of America

OCIS codes: 010.3640, 010.7030, 280.1100, 280.3640, 290.1350, 290.2200.

1. Introduction

The European Aerosol Research Lidar Network to Establish an Aerosol Climatology (EARLINET) is a joint project of 22 groups of lidar scientists operating aerosol lidar systems at 24 stations over a large part of Europe plus one group that is focusing on the mathematical problems associated with the retrieval of aerosol properties from lidar observations and one group using a regional atmospheric dust model to simulate all major phases of aerosol desert dust in the atmosphere as well as to validate the model's results compared with lidar observations. The last three groups named in Table 1, namely, those abbreviated ng, sf, and be in this paper got the opportunity to join the project only in 2002 because of political changes concerning the European Union. The main goal of EARLINET is to establish a comprehensive statistically representative data set of the aerosol vertical distribution. For this purpose, each lidar group performs vertical aerosol soundings on a routine basis three times a week on preselected days and times. Additionally, several special measurements, e.g., of Saharan dust, temporal cycles, rural and urban differences, and long- and medium-range transport, are part of the project.[1]

Most of the lidar systems transmit at least two wavelengths between UV and the near-IR spectral regions. A large number of systems are also equipped with Raman channels to detect the inelastic Raman backscattering from nitrogen molecules for deriving quantitative aerosol extinction profiles.[2]

Homogeneous and well-established data are key prerequisites for the use of combined data that originate from different systems. Because the establishment of a joint data set and its use in comparative studies are major objectives of EARLINET, specific attention is given to data quality assurance.

Besides instrument intercomparison,[3] a basic exercise to ensure the quality of network measurements is the comparison of the algorithms that are used to calculate the optical parameters from lidar signals. The importance of such comparisons was shown and proved in publications that described similar networks[4–6] and was accepted by the public at various conferences.[7,8]

Therefore intercomparisons of algorithms for retrieval as applied by different lidar groups were organized as part of the European Lidar Network. Retrieval of the particle backscatter-coefficient profile from a backscatter lidar is treated in detail in this paper. The retrieval of the particle extinction-coefficient profile from a Raman lidar was considered briefly in Ref. 9 and will be proposed in more detail in Ref. 10, i.e., in Part 3 of this series of paper.

In Section 2 we briefly describe the well-known retrieval method as it is applied to backscatter lidar data. In Section 3, procedures for evaluation and data simulation are shown. In Section 4 the results of the intercomparison study are discussed, and finally some conclusions are given.

2. Method of Backscatter-Coefficient Retrieval from Lidar Signals

The basis of any lidar signal analysis is the lidar equation that describes the receiver signal as a function of atmospheric and system parameters. The lidar equation in its simplest form is valid for quasi-monochromatic emission of the laser light, instantaneous scattering, and negligible multiple scattering and coherence:

$$P(\lambda, z) = P_0(\lambda)C \frac{O(z)}{z^2} \beta(\lambda, z)$$

$$\times \exp\left[-2 \int_0^z \alpha(\lambda, \zeta)d\zeta\right], \qquad (1)$$

where $P(\lambda, z)$ is the backscattered laser power at wavelength λ from range z and $P_0(\lambda)$ is the emitted laser power at wavelength λ. C is the range-independent system constant and $O(z)$ is the overlap function. $\beta(\lambda, z)$ stands for the backscatter coefficient and $\alpha(\lambda, \zeta)$ is the total extinction coefficient. $C = \eta A c \tau_L / 2$ depends on efficiency η of the detector system, receiving telescope area A, and pulse width of the laser τ_L. The speed of light is c.

Different methods can be applied to derive aerosol vertical profiles from lidar measurements. If only elastically backscattered light at one laser wavelength is available, aerosol backscatter profiles can be calculated only if assumptions are made about the relation between aerosol extinction and backscatter coefficients (lidar ratio) and for the backscatter coefficient at a calibration range. Because there is poor *a priori* knowledge of the lidar ratio and its profile, we show in this paper and in the companion paper[3] (Part 1) that the largest uncertainty in retrieving comes from the estimation of the lidar ratio. However, this type of lidar device is widely used because single-wavelength backscatter lidars are the systems that are easiest to operate and because it is at least a by-product of any lidar measurement.

Table 1. Participating Lidar System Groups and Capabilities of Their Processing Algorithms[a]

Abbreviated Name of Group[b]	Lidar Group	Lidar Ratio	Integration Direction	Radiosonde
ab	Department of Physics, University of Wales, Aberystwyth, United Kingdom	Yes	Yes	Yes
at	Department of Physics, National Technical University of Athens, Athens, Greece	Yes	No	No
ba	Universitat Politècnica de Catalunya, Barcelona, Spain	Yes	No	No
be	Institute of Geophysics, Polish Academy of Sciences, Warsaw, Poland	Yes	Yes	Yes
gp	Institut für Meteorologie und Klimaforschung, Garmisch-Partenkirchen, Germany	Yes	Yes	No
hh	Max-Planck-Institut für Meteorologie, Hamburg, Germany	Yes	Yes	Yes
ju	École Polytechnique Fédérale de Lausanne, Lausanne, Switzerland	Yes	Yes	Yes
kb	Leibniz-Institut für Atmosphärenphysik, Kühlungsborn, Germany	Yes	Yes	Yes
la	Departimento di Fisica, Università degli Studi, L'Aquila, Italy	Yes	Yes	Yes
lc	Istituto Nazionale per la Fisica della Materia, Dipartimento di Fisica, Universitá di Lecce, Lecce, Italy	Yes	Yes	Yes
le	Institute for Tropospheric Research, Leipzig, Germany	Yes	Yes	Yes
li	Centro de Física de Plasmas, Instituto Superior Técnico, Lisbon, Portugal	Yes	Yes	Yes
lk	Division of Sensor Technology, Linköping, Sweden	Yes	Yes	Yes
mi	Institute of Physics, National Academy of Sciences, Minsk, Belarus	Yes	Yes	Yes
mu	Meteorologisches Institut der Universität München, Munich, Germany	Yes	Yes	Yes
na	Istituto Nazionale per la Fisica della Materia, Complesso Universitario di Monte S. Angelo, Naples, Italy	Yes	Yes	Yes
ne	Observatoire de Neuchâtel, Neuchâtel, Switzerland	Yes	Yes	Yes
ng	Laboratory for Astroparticle Physics, Nova Gorica Polytechnic, Nova Gorica, Slovenia	Yes	Yes	Yes
pl	Institute Pierre Simone Laplace, Palaiseau Cedex, France	Yes	Yes	Yes
po	Istituto di Metodologie per l'Analisi Ambientale, Potenza, Italy	Yes	Yes	Yes
sf	Institute of Electronics, Bulgarian Academy of Sciences, Sofia, Bulgaria	Yes	No	Yes
th	Laboratory of Atmospheric Physics, University of Thessaloniki, Greece	Yes	Yes	Yes

[a]Height-dependent lidar ratio, both integration directions from the calibration point, and the possibility of including radiosonde data.
[b]The abbreviations for the lidar groups used here are the same ones that are used in the EARLINET data base.

To solve the lidar equation for one wavelength in the simplest case of no gaseous absorption it is useful to split backscatter and extinction into their molecular and aerosol parts and to use only that part of the profile at which the laser beam fully overlaps the field of view of the receiving telescope, i.e., $O(z) = 1$:

$$P(\lambda, z) = P_0(\lambda)C \frac{\beta_{aer}(\lambda, z) + \beta_{mol}(\lambda, z)}{z^2}$$
$$\times \exp\left[-2\int_0^z \alpha_{aer}(\lambda, \zeta) + \alpha_{mol}(\lambda, \zeta)d\zeta\right], \quad (2)$$

with the extinction coefficient

$$\alpha(\lambda, z) = \alpha_{mol}(\lambda, z) + \alpha_{aer}(\lambda, z)$$
$$= \alpha_{mol}^{abs}(\lambda, z) + \alpha_{mol}^{sca}(\lambda, z) + \alpha_{aer}^{abs}(\lambda, z)$$
$$+ \alpha_{aer}^{sca}(\lambda, z). \quad (3)$$

Assuming that the molecular part of Eq. (3) can be calculated by use of standard atmosphere conditions or an atmospheric density profile from radiosondes nearby launched, $\alpha_{aer}(z)$ and $\beta_{aer}(z)$ remain two height-dependent unknowns and only one signal has been measured. One usually solves this problem by assuming an (a priori unknown) relationship between aerosol backscatter and extinction. $S_{aer}(\lambda, z) = \alpha_{aer}(\lambda, z)/\beta_{aer}(\lambda, z)$ is usually called the lidar ratio. It is wavelength and height dependent. The determination of $\beta_{aer}(z)$ for one wavelength from Eq. (2) requires the additional assumption of an unknown constant that represents the height-independent system parameters. To solve the equation for $\beta_{aer}(z)$, usually a calibration or reference value $\beta_{aer}(\lambda, z_0)$ is chosen that prescribes the aerosol backscatter at a certain height z_0.

Under these assumptions, the equation for $\beta_{aer}(z)$ can be solved following the research of Klett,[11,12] Fernald et al.,[13] and Fernald,[14] using the notation

$$\beta_{aer}(z) = -\beta_{mol}(z) + \frac{P(z)z^2 \exp\left[-2(S_{aer} - S_{mol})\int_0^z \beta_{mol}(\zeta)d\zeta\right]}{P_0 C - 2S_{aer}\int_0^z P(\zeta)\zeta^2 \exp\left[-2(S_{aer} - S_{mol})\int_0^\zeta \beta_{mol}(z')dz'\right]d\zeta}, \quad (4)$$

where $S_{mol} = \alpha_{mol}(\lambda, z)/\beta_{mol}(\lambda, z) = 8\pi/3$. Calibration in height z_0 gives system constants $P_0(\lambda)C$. Writing $X(z) = P(z)z^2$ gives

Stage 2: The prescribed lidar ratio profile was provided to all groups. The evaluation was repeated.

$$
\beta_{aer}(z) = -\beta_{mol}(z) + \frac{X(z)\exp\left[-2(S_{aer} - S_{mol})\int_{z_0}^{z}\beta_{mol}(\zeta)d\zeta\right]}{X(z_0)/[\beta_{aer}(z_0) + \beta_{mol}(z_0)] - 2S_{aer}\int_{z_0}^{z}X(\zeta)\exp\left[-2(S_{aer} - S_{mol})\int_{z_0}^{\zeta}\beta_{mol}(z')dz'\right]d\zeta}. \quad (5)
$$

Equation (5) can then be solved iteratively downward or upward from z_0. It is advantageous with respect to the error propagation to chose a height $z_0 > z$, i.e., to use calibration in the far range. Molecular absorption is neglected here. Molecular scattering can be calculated from

$$
\alpha_{mol}{}^{sca}(z, \lambda; p, T) = \frac{24\pi^3(m_{air}{}^2 - 1)^2}{\lambda^4 N_S{}^2(m_{air}{}^2 + 2)^2}\frac{6 + 3\gamma}{6 - 7\gamma}
$$
$$
\times N_S\frac{T_0}{p_0}\frac{p(z)}{T(z)}, \quad (6)
$$

with refractive index of the air m_{air}, depolarization factor[15] γ (γ is 0.0301, 0.0284, and 0.0273 for 350, 550, and 1000 nm, respectively), and molecular number density $N_s = 2.547 \times 10^{19}$ cm^{-3} for standard atmospheric conditions at ground level ($p_0 = 1013.25$ hPa, $T_0 = 15$ °C). Profiles of temperature $T(z)$ and pressure $p(z)$ are taken from actual radiosonde measurements or from a standard atmosphere[16,17] with actual ground values of temperature and pressure. We emphasize once again that two unknown quantities, the particle lidar ratio and the particle backscatter coefficient $\beta_{aer}(z_0)$ at a suitable reference height z_0, have to be estimated in the determination of the particle backscatter-coefficient profile after Eq. (5). The numerical application of Eq. (5) have been discussed in the literature, identified as the Fernald or the Klett algorithm, for more than 20 years. Contributions to solving the problem are also given in Refs. 18–21. All those improvements are usually considered in the individual algorithms constructed by the various lidar groups.

3. Evaluation Procedure and Data Simulation

Determination of the particle backscatter coefficient from a single elastic backscatter signal was investigated as part of our intercomparison of algorithms.

The procedure for the algorithm intercomparison was divided into three stages. Stage 1 is the hardest one because the degree of *a priori* knowledge available before the retrieval is smallest. The three stages were as follows:

Stage 1: The simulated signals, without any information on the input parameters except on the standard atmosphere used, were distributed to all groups. Each group calculated particle backscatter coefficient profiles, using its own algorithm.

Stage 3: The reference value at calibration height was also provided. The evaluation was repeated.

For each stage the results were collected and evaluated by numerical group at the Institute of Mathematics of the Potsdam University, Germany because this group is not involved in experimental lidar work and acted as the referee. The first stage was the most difficult but also the most realistic one, because at that stage lidar-ratio profiles and reference values were unknown. Therefore, not only the correctness and accuracy of the algorithms but also the dependence of the solution on estimates of the lidar ratio and on the reference value were proved. In the third and final stage all parameters were known. So the numerical correctness and stability of the algorithms were definitely tested.

Three cases were developed for the major algorithm intercomparison. Therefore all participating groups, whose names and initials are listed in Table 1, except groups be, li, ng, and sf, processed three sets of synthetic lidar data, using their individual algorithms. Some specific details of the groups' individual algorithms are presented in Table 1. Thereby, synthetic lidar signals were used to test the numerical correctness and accuracy of the algorithms as well as the experience of the groups and the limits of the method itself. The three cases with different degrees of difficulty in solving for the backscatter coefficients were calculated with the lidar simulation model of the Institute of Tropospheric Research, Leipzig, Germany.

The simulations were performed by a person who was not involved in the evaluation of these data for the intercomparison study, and the input data were not known to other persons. The Institute of Tropospheric Research's software permits simulation and evaluation, elastically and inelastically, of the dependence of backscattered lidar signals at arbitrary wavelengths on a variety of system parameters for a variable model atmosphere with arbitrary aerosol and cloud layers. Sky background, background noise, and signal noise are considered as well. Atmospheric input parameters are profiles of temperature and pressure used in calculating Rayleigh scattering and profiles of extinction coefficients and lidar ratios for the simulation of aerosol and cloud layers.

In more detail, three different data sets of elastic backscatter signals at wavelengths of 355, 532, and 1064 nm were simulated. A U.S. standard atmo-
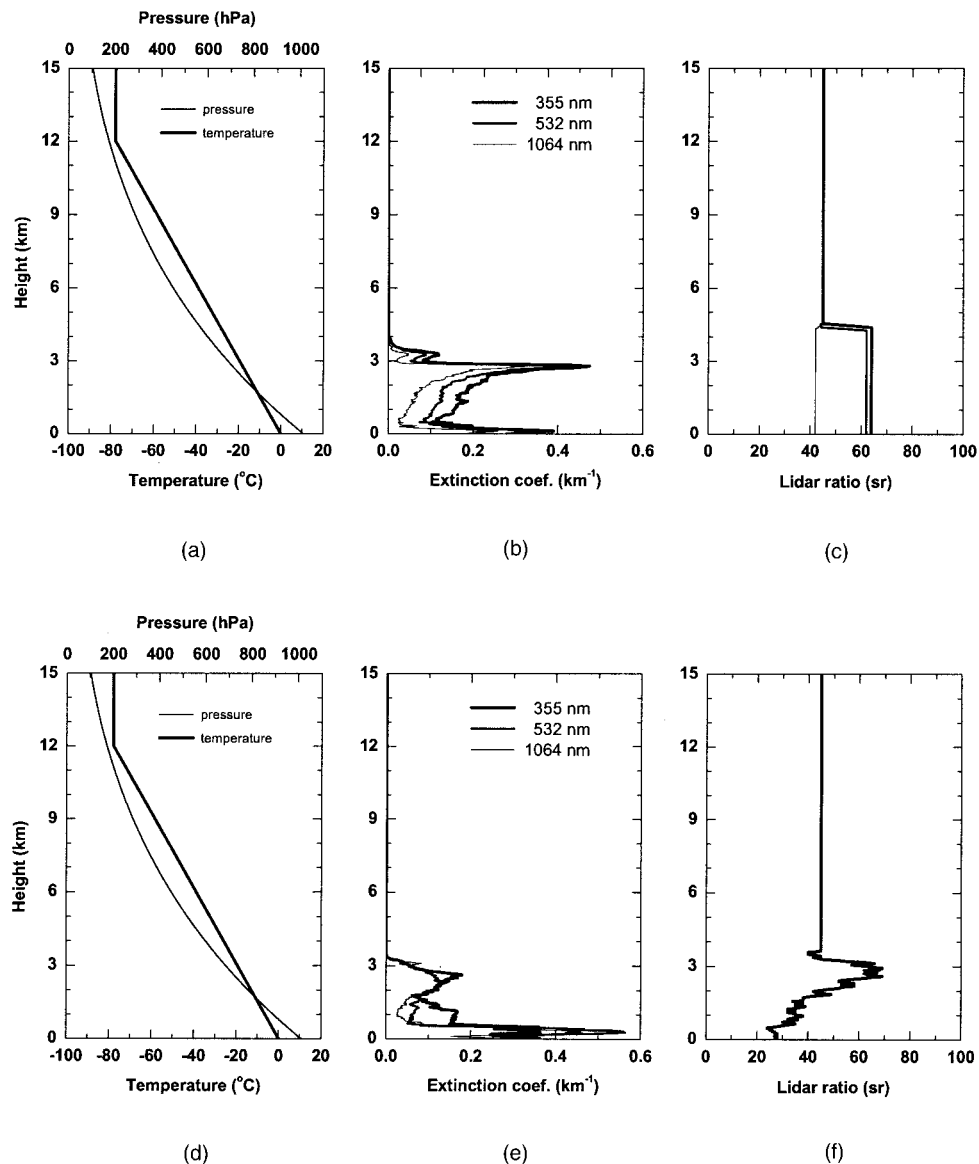
Fig. 1. Input data for (a)–(c) simulation case 2 and (d)–(f) simulation case 3. In case 3 all wavelengths have the same lidar ratio profile.

sphere[22] with a ground pressure of 1013 hPa and a ground temperature of 0 °C, a tropopause height of 12.0 km, and the isothermal conditions over this layer was assumed. The signal profiles were simulated without signal noise. An incomplete overlap of laser beam and receiver field of view below 250 m was introduced. The simulation of the incomplete overlap should remind the experimenters that one has to take great care when one is working in the nearest range to the lidar, i.e., 100 m to several hundreds of meters, where the overlap function is generally not well known, even if a correction is applied for; see Ref. 23. Typical system parameters, e.g., laser power and telescope diameter, were used for the calculations. However, they are not of importance for the algorithm intercomparison.

In all cases, only boundary-layer aerosols at heights below 4.5 km were simulated. Minor particle scattering in the free troposphere and the strato-

sphere was introduced, and no clouds were considered. The three simulation cases represent different atmospheric conditions with increasing degrees of difficulty in data evaluation:

Case 1: The first case did not represent realistic atmospheric conditions. The extinction coefficient was independent of wavelength and changed stepwise from 3×10^{-4} m^{-1} below 1500 m to 3.5×10^{-4} m^{-1} at 1500–2000 m and to 4×10^{-4} m^{-1} at 2000–2440 m and decreased to values below 10^{-6} m^{-1} over 2440 m. The lidar ratio had a constant value of 50 sr for all heights and all wavelengths.

Case 2: In the second case a significant aerosol load up to 4000 m was simulated [see Figs. 1(a)–1(c). A more realistic, height-dependent extinction coefficient was assumed. In addition, the extinction coefficient changed with wavelength, with highest values for the shortest wavelength and lowest values for the

Table 2. Mean Errors with Standard Deviations of Cases 2 and 3 for Wavelength 355 nm in Stage 3

Lidar System Group	Case 2		Case 3	
	Mean Relative Error at 0.3075–3.4875 km (%)	Mean Absolute Error at 3.5025–15.0675 km $(\text{km}^{-1}\,\text{sr}^{-1})$	Mean Relative Error at 0.3075–3.0075 km (%)	Mean Absolute Error at 3.0225–15.0675 km $(\text{km}^{-1}\,\text{sr}^{-1})$
ab	1.76 ± 1.05	$5.01 \times 10^{-6} \pm 4.27 \times 10^{-6}$	0.72 ± 0.47	$5.07 \times 10^{-6} \pm 3.81 \times 10^{-6}$
at	3.73 ± 5.65	$8.76 \times 10^{-7} \pm 2.56 \times 10^{-6}$	1.39 ± 1.45	$1.92 \times 10^{-6} \pm 4.73 \times 10^{-6}$
ba	0.90 ± 0.80	$6.73 \times 10^{-5} \pm 3.76 \times 10^{-5}$	0.96 ± 0.72	$6.53 \times 10^{-5} \pm 3.81 \times 10^{-5}$
gp	4.82 ± 1.85	$4.41 \times 10^{-5} \pm 1.71 \times 10^{-5}$	3.76 ± 2.14	$3.15 \times 10^{-5} \pm 2.58 \times 10^{-5}$
hh	1.84 ± 2.14	$3.91 \times 10^{-6} \pm 2.59 \times 10^{-6}$	1.51 ± 0.79	$4.14 \times 10^{-6} \pm 3.15 \times 10^{-6}$
ju	1.54 ± 0.91	$1.72 \times 10^{-5} \pm 1.28 \times 10^{-5}$	1.01 ± 0.85	$1.85 \times 10^{-5} \pm 1.41 \times 10^{-5}$
kb	0.46 ± 0.40	$2.59 \times 10^{-7} \pm 5.20 \times 10^{-7}$	0.63 ± 0.28	$3.43 \times 10^{-7} \pm 1.22 \times 10^{-6}$
la	0.46 ± 0.40	$1.41 \times 10^{-7} \pm 5.36 \times 10^{-7}$	0.63 ± 0.28	$2.34 \times 10^{-7} \pm 1.22 \times 10^{-6}$
lc	0.45 ± 0.40	$2.95 \times 10^{-7} \pm 5.76 \times 10^{-7}$	0.63 ± 0.28	$9.31 \times 10^{-7} \pm 2.17 \times 10^{-6}$
le	0.45 ± 0.38	$3.94 \times 10^{-7} \pm 5.42 \times 10^{-7}$	0.60 ± 0.30	$4.94 \times 10^{-7} \pm 1.14 \times 10^{-6}$
lk	3.66 ± 0.62	$6.65 \times 10^{-6} \pm 4.85 \times 10^{-6}$	3.11 ± 0.72	$6.46 \times 10^{-6} \pm 5.64 \times 10^{-6}$
mi	0.45 ± 0.41	$4.27 \times 10^{-7} \pm 6.52 \times 10^{-7}$	0.68 ± 0.47	$5.41 \times 10^{-7} \pm 1.34 \times 10^{-6}$
mu	2.45 ± 1.56	$2.79 \times 10^{-5} \pm 2.08 \times 10^{-5}$	1.58 ± 1.32	$2.99 \times 10^{-5} \pm 2.26 \times 10^{-5}$
na	2.25 ± 1.21	$2.28 \times 10^{-5} \pm 1.71 \times 10^{-5}$	1.86 ± 1.21	$2.44 \times 10^{-5} \pm 1.86 \times 10^{-5}$
ne	0.46 ± 0.40	$1.43 \times 10^{-7} \pm 5.42 \times 10^{-7}$	0.63 ± 0.29	$2.38 \times 10^{-7} \pm 1.24 \times 10^{-6}$
pl	0.48 ± 0.42	$2.32 \times 10^{-6} \pm 1.42 \times 10^{-6}$	12.88 ± 8.27	$7.44 \times 10^{-6} \pm 1.40 \times 10^{-5}$
po	2.25 ± 1.21	$2.28 \times 10^{-5} \pm 1.71 \times 10^{-5}$	1.86 ± 1.21	$2.44 \times 10^{-5} \pm 1.86 \times 10^{-5}$
th	5.57 ± 3.25	$2.18 \times 10^{-5} \pm 4.62 \times 10^{-5}$	5.34 ± 3.86	$2.89 \times 10^{-5} \pm 5.67 \times 10^{-5}$
Mean values	1.87	1.30×10^{-5}	2.23	1.33×10^{-5}

longest wavelength. The lidar ratio was height independent in the aerosol layer but took values of 64 sr for 355 nm, 62 sr for 532 nm, and 42 sr for 1064 nm. Above 4500 m the lidar ratio was 45 sr for all wavelengths.

Case 3: In case 3 a significant aerosol load up to 3300 m was simulated [see Figs. 1(d)–1(f)]. Realistic, height-dependent extinction coefficients and lidar ratios were introduced. The extinction coefficient varied widely with wavelength at different heights. The lidar ratio took values of 24–69 sr but did not vary with wavelength. Above 3600 m the lidar ratio was set to 45 sr for all wavelengths.

Case 4: Case 4 comprises an additional situation for the lidar groups that joined the EARLINET community later, as mentioned above. The major intercomparison was already finished, and all results were known to the whole community. Therefore an entirely different test had to be used. It will be discussed only briefly. In case 4 a realistic EARLINET evening winter measurement in central Europe near sunset without clouds but with a dominating high-

Table 3. Mean Errors with Standard Deviations of Cases 2 and 3 Wavelength 532 nm in Stage 3

Lidar System Group	Case 2		Case 3	
	Mean Relative Error at 0.3075–3.4875 km (%)	Mean Absolute Error at 3.5025–15.0675 km $(\text{km}^{-1}\,\text{sr}^{-1})$	Mean Relative Error at 0.3075–3.0075 km (%)	Mean Absolute Error at 3.0225–15.0675 km $(\text{km}^{-1}\,\text{sr}^{-1})$
ab	0.63 ± 0.46	$1.98 \times 10^{-7} \pm 7.77 \times 10^{-7}$	0.90 ± 0.25	$3.57 \times 10^{-7} \pm 1.70 \times 10^{-6}$
at	0.71 ± 0.48	$1.80 \times 10^{-7} \pm 5.69 \times 10^{-7}$	1.17 ± 3.35	$2.97 \times 10^{-7} \pm 1.28 \times 10^{-6}$
ba	4.54 ± 2.78	$3.44 \times 10^{-5} \pm 1.53 \times 10^{-5}$	5.45 ± 1.78	$3.49 \times 10^{-5} \pm 1.67 \times 10^{-5}$
gp	5.22 ± 2.73	$1.92 \times 10^{-5} \pm 1.15 \times 10^{-5}$	6.39 ± 1.73	$1.45 \times 10^{-5} \pm 1.65 \times 10^{-5}$
hh	2.34 ± 1.07	$9.97 \times 10^{-7} \pm 1.39 \times 10^{-6}$	2.24 ± 0.66	$1.29 \times 10^{-6} \pm 2.96 \times 10^{-6}$
ju	0.91 ± 0.72	$9.68 \times 10^{-7} \pm 1.00 \times 10^{-6}$	1.36 ± 0.39	$1.24 \times 10^{-6} \pm 1.80 \times 10^{-6}$
kb	0.72 ± 0.46	$1.75 \times 10^{-7} \pm 6.20 \times 10^{-7}$	0.98 ± 0.24	$2.74 \times 10^{-7} \pm 1.36 \times 10^{-6}$
la	0.71 ± 0.46	$1.13 \times 10^{-7} \pm 6.12 \times 10^{-7}$	0.97 ± 0.23	$2.11 \times 10^{-7} \pm 1.34 \times 10^{-6}$
lc	0.70 ± 0.44	$1.27 \times 10^{-7} \pm 6.04 \times 10^{-7}$	0.95 ± 0.23	$2.14 \times 10^{-7} \pm 1.31 \times 10^{-6}$
le	0.62 ± 0.47	$2.24 \times 10^{-7} \pm 4.92 \times 10^{-7}$	0.88 ± 0.28	$3.32 \times 10^{-7} \pm 1.14 \times 10^{-6}$
lk	–	–	–	–
mi	0.68 ± 0.43	$1.23 \times 10^{-7} \pm 5.92 \times 10^{-7}$	0.94 ± 0.23	$2.16 \times 10^{-7} \pm 1.28 \times 10^{-6}$
mu	0.16 ± 0.14	$4.90 \times 10^{-7} \pm 4.61 \times 10^{-7}$	0.19 ± 0.08	$5.34 \times 10^{-7} \pm 5.04 \times 10^{-7}$
na	1.36 ± 0.82	$3.98 \times 10^{-7} \pm 1.24 \times 10^{-6}$	1.84 ± 0.44	$5.95 \times 10^{-7} \pm 2.57 \times 10^{-6}$
ne	0.71 ± 0.46	$1.16 \times 10^{-7} \pm 6.13 \times 10^{-7}$	0.97 ± 0.23	$2.12 \times 10^{-7} \pm 1.33 \times 10^{-6}$
pl	0.81 ± 0.52	$2.28 \times 10^{-6} \pm 1.91 \times 10^{-6}$	8.18 ± 2.88	$4.36 \times 10^{-6} \pm 7.19 \times 10^{-6}$
po	1.36 ± 0.82	$3.98 \times 10^{-7} \pm 1.24 \times 10^{-6}$	1.84 ± 0.44	$5.95 \times 10^{-7} \pm 2.57 \times 10^{-6}$
th	2.90 ± 1.59	$5.54 \times 10^{-6} \pm 1.22 \times 10^{-5}$	2.88 ± 3.41	$7.31 \times 10^{-6} \pm 5.30 \times 10^{-6}$
Mean values	1.48	4.10×10^{-6}	2.27	4.18×10^{-6}

Table 4. Mean Errors with Standard Deviations of Cases 2 and 3 for Wavelength 1064 nm in Stage 3

Lidar System Group	Case 2 Mean Relative Error at 0.3075–3.4875 km (%)	Case 2 Mean Absolute Error at 3.5025–15.0675 km ($km^{-1}\,sr^{-1}$)	Case 3 Mean Relative Error at 0.3075–3.0075 km (%)	Case 3 Mean Absolute Error at 3.0225–15.0675 km ($km^{-1}\,sr^{-1}$)
ab	0.19 ± 0.04	$1.34 \times 10^{-8} \pm 6.28 \times 10^{-8}$	0.19 ± 0.03	$7.77 \times 10^{-8} \pm 4.28 \times 10^{-7}$
at	–	–	–	–
ba	6.42 ± 1.48	$3.05 \times 10^{-6} \pm 2.40 \times 10^{-6}$	6.25 ± 0.87	$4.21 \times 10^{-6} \pm 1.05 \times 10^{-5}$
gp	0.66 ± 0.27	$1.19 \times 10^{-6} \pm 7.53 \times 10^{-7}$	0.83 ± 1.72	$1.14 \times 10^{-6} \pm 3.33 \times 10^{-6}$
hh	1.94 ± 0.85	$1.01 \times 10^{-7} \pm 3.29 \times 10^{-7}$	1.57 ± 0.55	$3.57 \times 10^{-7} \pm 2.16 \times 10^{-6}$
ju	2.88 ± 0.60	$1.18 \times 10^{-7} \pm 7.29 \times 10^{-7}$	3.05 ± 0.39	$7.02 \times 10^{-7} \pm 5.10 \times 10^{-6}$
kb	0.22 ± 0.05	$1.36 \times 10^{-8} \pm 5.59 \times 10^{-8}$	0.23 ± 0.03	$5.80 \times 10^{-8} \pm 3.86 \times 10^{-7}$
la	0.22 ± 0.04	$8.89 \times 10^{-9} \pm 5.35 \times 10^{-8}$	0.22 ± 0.03	$5.13 \times 10^{-8} \pm 3.72 \times 10^{-7}$
lc	0.23 ± 0.05	$9.25 \times 10^{-9} \pm 5.61 \times 10^{-8}$	0.23 ± 0.03	$5.42 \times 10^{-8} \pm 3.93 \times 10^{-7}$
le	0.15 ± 0.11	$1.54 \times 10^{-8} \pm 4.81 \times 10^{-8}$	0.17 ± 0.12	$4.95 \times 10^{-8} \pm 3.99 \times 10^{-7}$
lk	–	–	–	–
mi	0.19 ± 0.04	$9.86 \times 10^{-9} \pm 4.63 \times 10^{-8}$	0.21 ± 0.04	$4.95 \times 10^{-8} \pm 3.51 \times 10^{-7}$
mu	1.29 ± 0.27	$5.25 \times 10^{-8} \pm 3.19 \times 10^{-7}$	1.38 ± 0.15	$3.08 \times 10^{-7} \pm 2.23 \times 10^{-6}$
na	3.44 ± 0.74	$1.37 \times 10^{-7} \pm 8.64 \times 10^{-7}$	3.56 ± 0.50	$8.31 \times 10^{-7} \pm 6.03 \times 10^{-6}$
ne	0.21 ± 0.04	$8.89 \times 10^{-9} \pm 5.31 \times 10^{-8}$	0.22 ± 0.03	$5.29 \times 10^{-8} \pm 3.75 \times 10^{-7}$
pl	1.31 ± 0.28	$1.51 \times 10^{-6} \pm 9.12 \times 10^{-7}$	8.33 ± 5.22	$4.35 \times 10^{-6} \pm 6.35 \times 10^{-6}$
po	3.44 ± 0.74	$1.37 \times 10^{-7} \pm 8.64 \times 10^{-7}$	3.56 ± 0.50	$8.31 \times 10^{-7} \pm 6.03 \times 10^{-6}$
th	–	–	–	–
Mean values	1.38	4.46×10^{-7}	1.89	8.78×10^{-7}

pressure system and a variable, visible, and stable aerosol layering up to 2000 m was simulated. Additionally, a Saharian dust layer, a weak aerosol layer at 3000–4500 m, was simulated. Whereas the lower layer showed a strong dependence of the extinction coefficient on wavelength, for the upper layer the dependence was slight. The lidar ratio was height and wavelength dependent in the aerosol layers but constant in each case over certain height ranges and took values of 48–79 and 40–65 sr, respectively, for 355 and 532 nm. The ground temperature was -2 °C; the ground pressure was 1025 hPa. The measurement lasted 30 min, and signal profiles were stored with 2-min and 15-m resolution. Moreover, a realistic signal noise, but no background noise, was simulated.

For the first case, which was the easiest one and is not discussed further here, the input profiles of extinction-coefficient and lidar ratio were provided to the participants to permit an exercise with known solutions. Cases 2–4 were used directly for the intercomparison, and the results are presented here.

We compared the retrieval solutions of each group from each stage and case with the input data to determine the systematic errors. The results are discussed in Section 4.

4. Intercomparison Results

The numerical schemes differ from one other only in some details. Before Eq. (5) can be applied to measured lidar signals, the signals are averaged over the time interval of interest, corrected for background, and usually spatially averaged, i.e., smoothed. For the synthetic data used here, this procedure was not necessary, except for case 4. In Table 1, details of

the individual algorithms are given to address the following questions:

• Is determination of the backscatter-coefficient profile with height-dependent lidar ratio S_{aer} possible?
• Is integration in Eq. (5) in forward and backward directions possible?
• Is it possible to use temperature and pressure values from a radiosonde ascent?

Tables 2–4 and Figs. 2–5 summarize the results of the algorithm intercomparison. In contrast to the specifications designated in Ref. 3, i.e., Part 1 of this series, here the quality criteria have to address checking the correctness and accuracy of a numerical algorithm in stage 3. Therefore positive and negative errors have to be penalized in the same manner. Additionally, here we compare the retrieved profiles and the exact profile. For these reasons, first, we use the term "error" instead of "deviation." Second, the absolute value of the differences must be compared. In detail, if the absolute difference or the relative difference between retrieved profile g_r and exact profile g_{ex} at a certain height is $\Delta g_{abs} = |g_r - g_{ex}|$ or

$$\Delta g_{rel} = \frac{\Delta g_{abs}}{g_{ex}} \times 100\%, \qquad (7)$$

respectively, then the mean absolute error or the mean relative error, respectively, is, as usual,

$$\overline{\Delta g_{abs/rel}} = \frac{\sum_{i=1}^{n} \Delta g_{abs/rel}}{n}, \qquad (8)$$
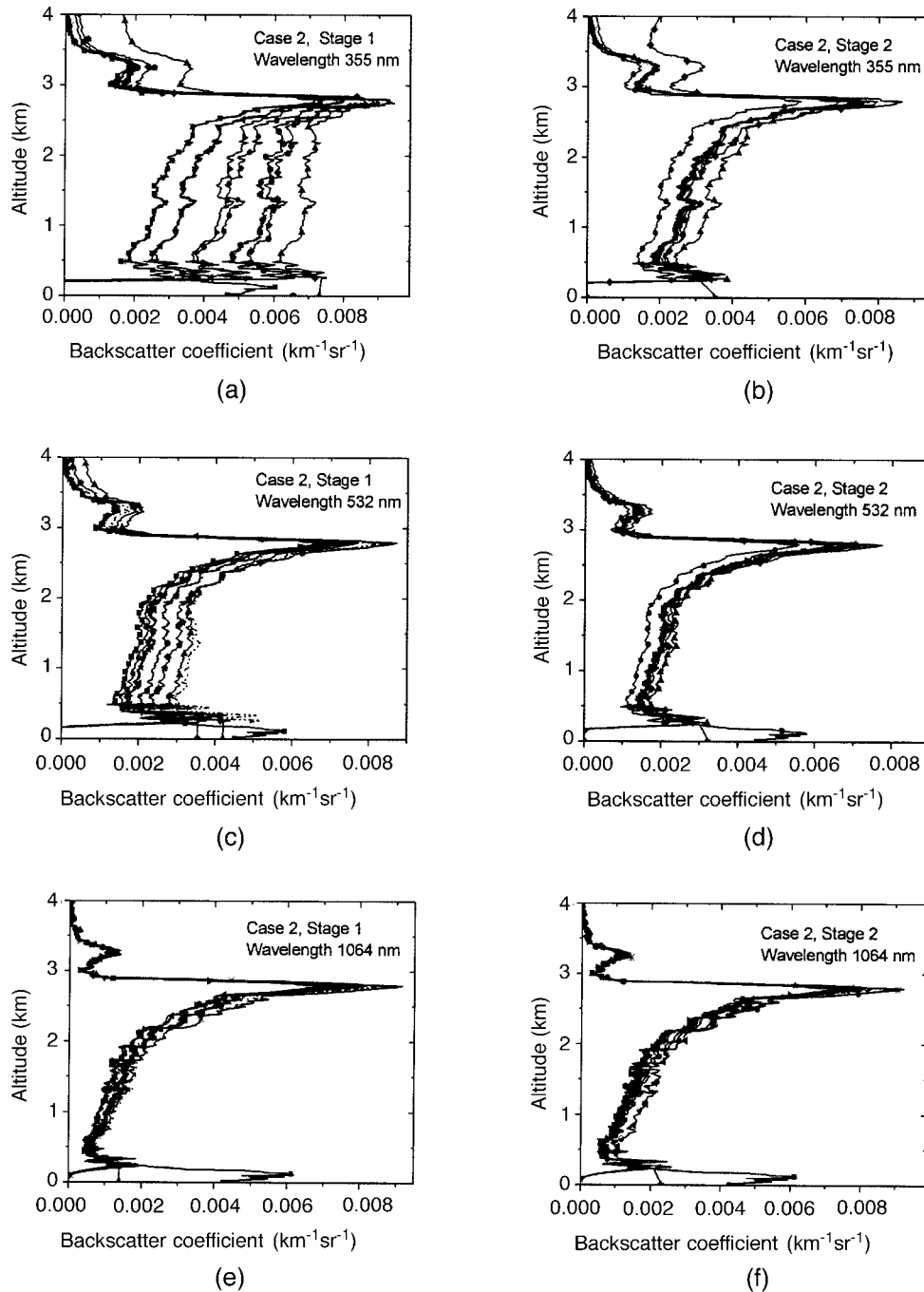
Fig. 2. Retrieved particle backscatter-coefficient profiles at all three wavelengths compared with the simulation input profiles of case 2 for (a), (c), (e) the first stage and (b), (d), (f) the second stage. The exact profile is included as a single curve with filled squares.

if n height values are compared. Finally, the standard deviation is calculated by

$$\delta g_{abs/rel} = \left[\frac{\sum\limits_{i=1}^{n} \left(\Delta g_{abs/rel} - \overline{\Delta g_{abs/rel}} \right)^2}{n} \right]^{1/2} . \quad (9)$$

The results for case 2 are shown in detail in Figs. 2 and 3 and are listed in columns 2 and 3 of Tables 2–4. In the first stage the mean relative errors from the exact solution (Fig. 2, left) were 0–120%.

Especially for wavelength 355 nm, the errors are very large, whereas with increasing wavelength the mean relative errors become smaller. The mean relative errors over all groups for wavelengths 355, 532, and 1064 nm are approximately 65%, 30%, and 15%, respectively. In the second stage with a known lidar-ratio profile but a still unknown reference value, the mean relative errors from the correct solution (Fig. 2, right) become visibly smaller and were approximately 0–30% only. The mean relative errors over all groups for the wavelengths
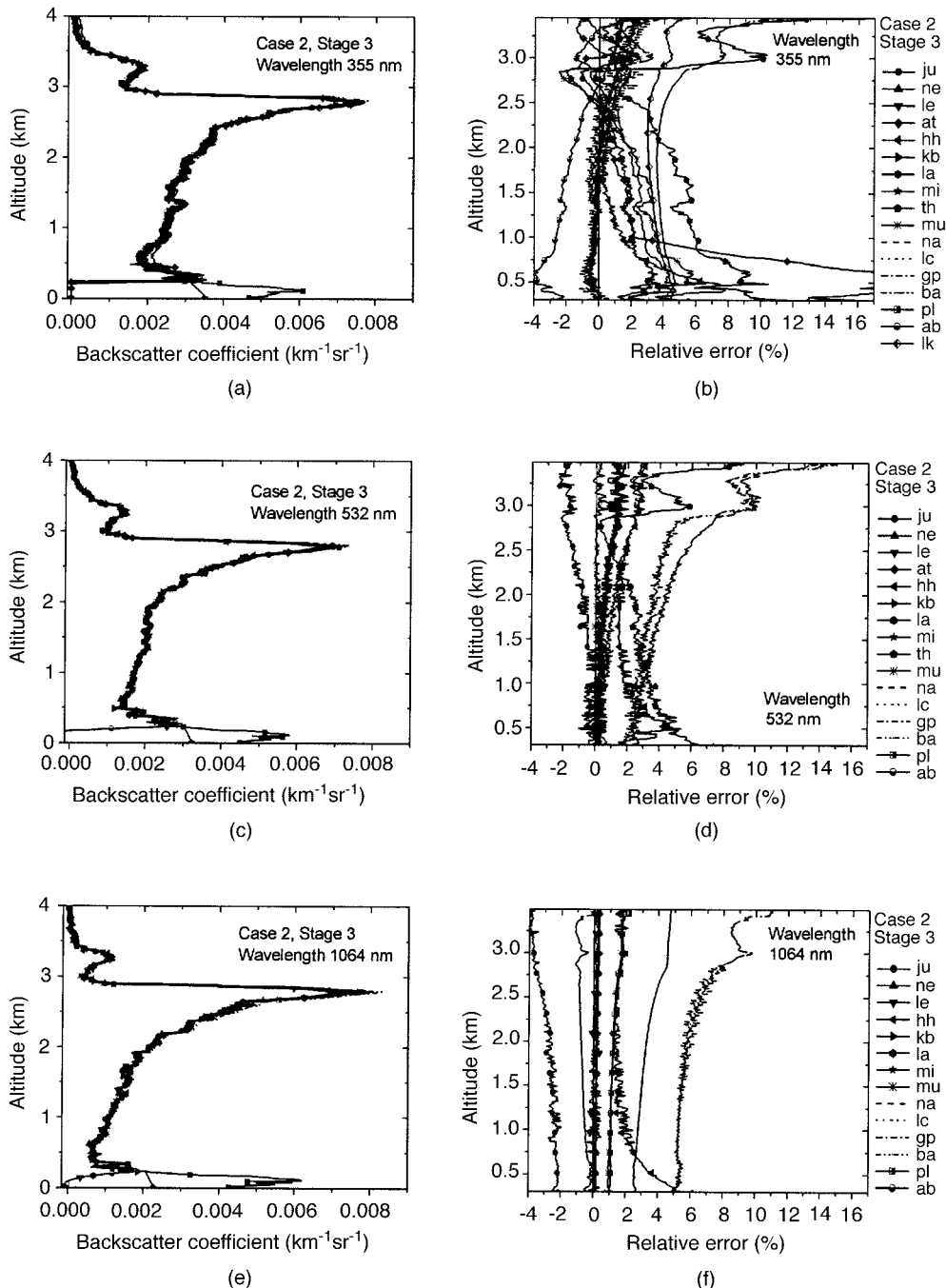
Fig. 3. Retrieved particle backscatter-coefficient profiles at all three wavelengths compared with (a), (c), (e) the simulation input profiles and (b), (d), (f) the respective relative errors of case 2 for the third stage.

355, 532, and 1064 nm are approximately 7%, 5%, and 8%, respectively.

Stage 2 represents the combined sunphotometer–lidar observations. The sunphotometer measures the particles' optical depth, which can be used as a constraint in retrieval of the profile of the backscatter coefficient. The ratio of optical depth to column-integrated backscatter yields the column lidar ratio. Thus the most appropriate range-independent lidar ratio is known.

The final stage for case 2 is shown in Fig. 3 in more

detail, including relative error profiles with sign. First, with increasing knowledge of the input parameters in stages 2 and 3, the mean relative errors decreased to a few percent, well below 5%, within the range 0.3075–3.4875 km. This is true for all wavelengths in almost all individual algorithms; see Fig. 3 and Tables 2–4. The mean relative error over all groups stays well below 2% for all wavelengths. Second, in the range from 3.5025 to 15.0675 km the mean absolute error over all groups is less than 1×10^{-5} $(km \ sr)^{-1}$. Both facts indicate that all algo-
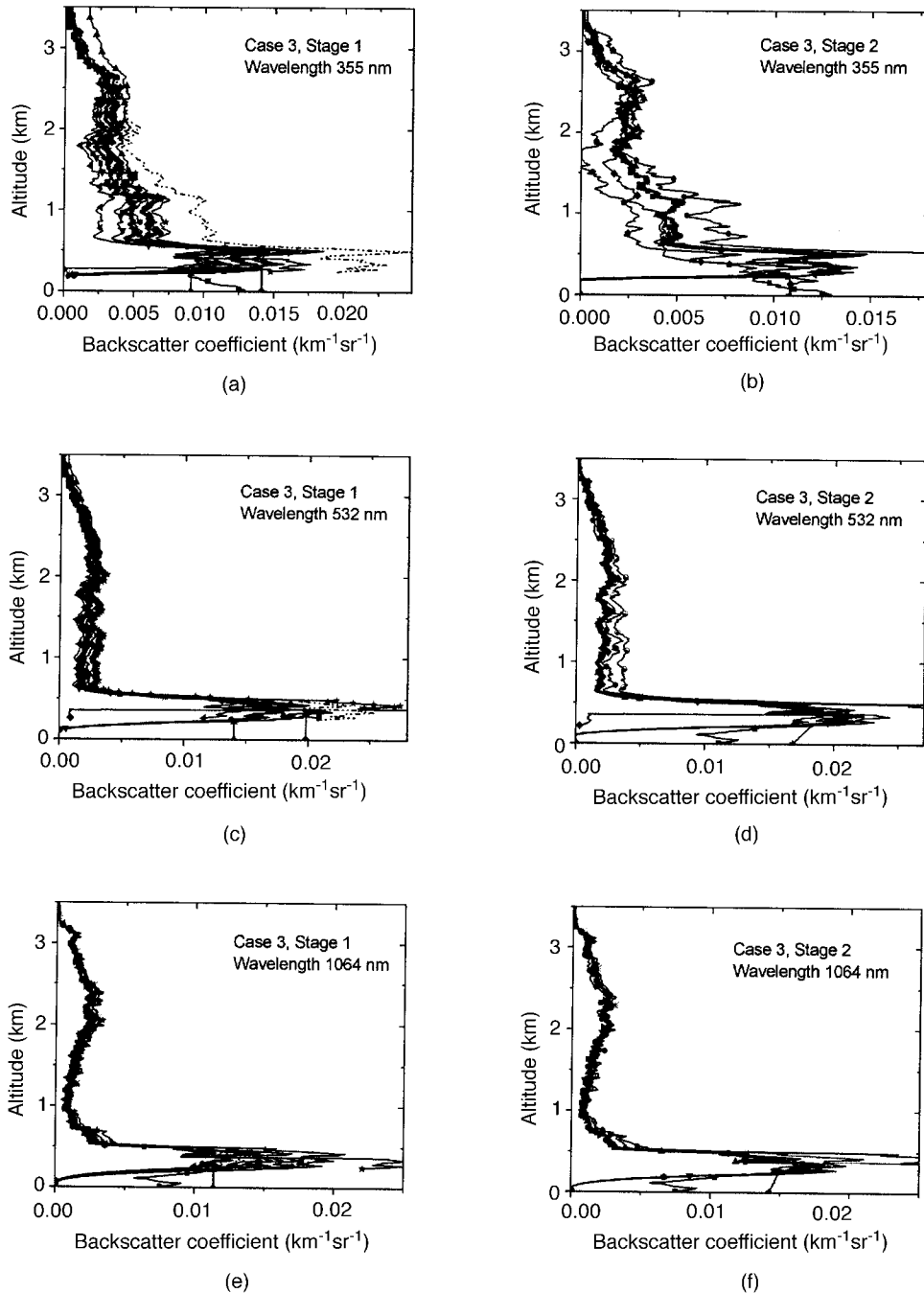
Fig. 4. Retrieved particle backscatter-coefficient profiles at all three wavelengths compared with the simulation input profiles of case 3 for (a), (c), (e) the first stage and (b), (d), (f) the second stage.

rithms work well and can generally reproduce the simulated profiles of case 2 if all input parameters are known.

Finally, it can be seen from the figures that the overlap effect in the lowest 250 m introduces large errors. As mentioned above, great care has to be exercised in the interpretation of data in the range nearest the lidar.

The results for case 3, which is more realistic, with a height-dependent lidar ratio but still without statistical noise and without clouds, are shown in Figs.

4 and 5 and in columns 4 and 5 of Tables 2–4. For stages 1 and 2 the mean errors are more-or-less in the same range as for case 2. In detail, the mean relative errors over all groups for the first stage for wavelengths of 355, 532, and 1064 nm are approximately 40%, 20%, and 17%, respectively. Moreover, for stage 2 the respective mean relative errors are approximately 10%, 8%, and 7%. For the third stage, the errors are somewhat larger than for case 2 and are caused mainly by the height-dependent lidar ratio. In the range 0.3075–3.0075 km (Fig. 5 and Ta-
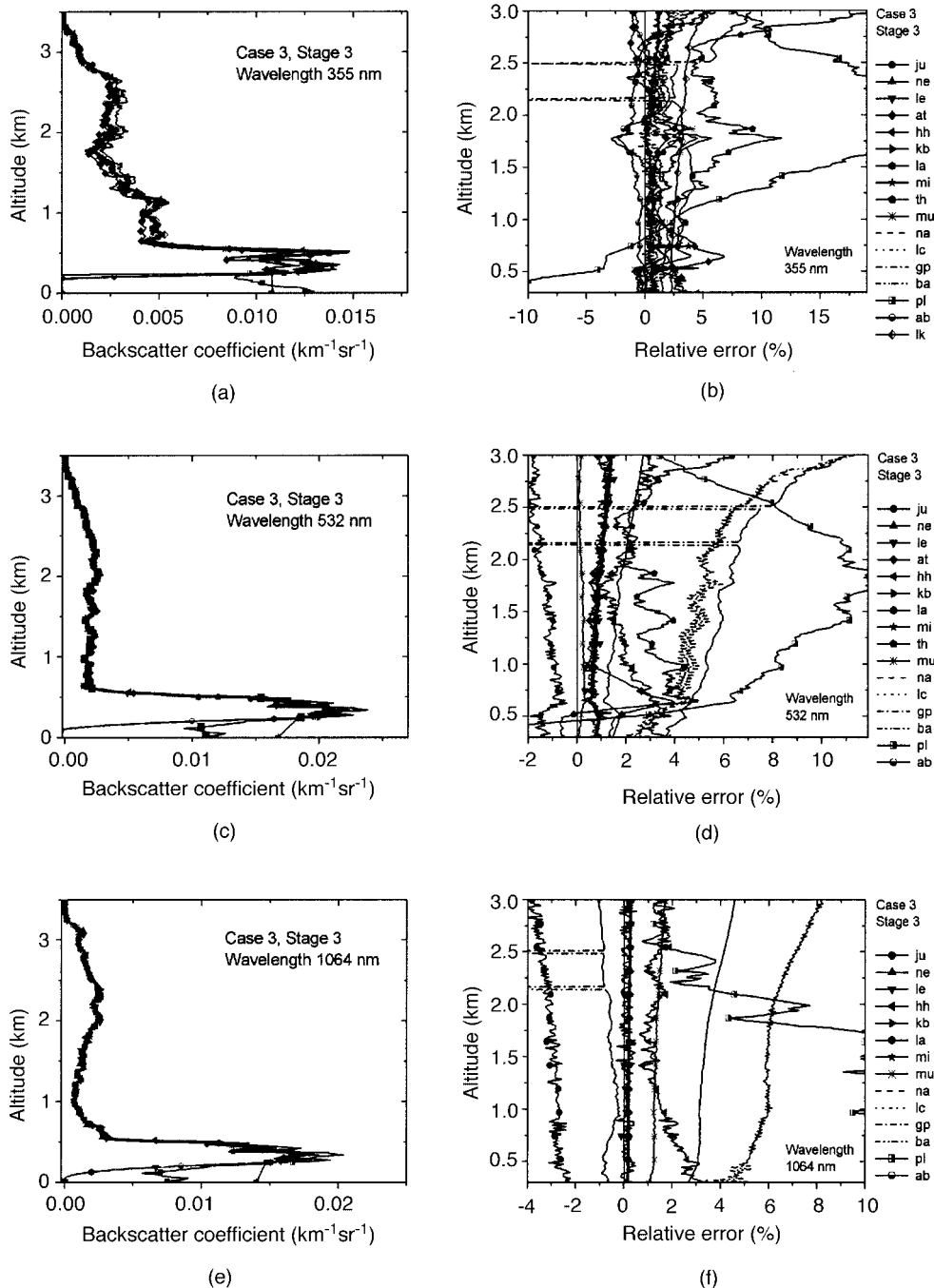
Fig. 5. Retrieved particle backscatter-coefficient profiles at all three wavelengths compared with (a), (c), (e) the simulation input profiles and (b), (d), (f) the respective relative errors for case 3 for the third stage.

bles 2–4) the mean relative error over all groups stays well below 3% for all wavelengths. Only the French group abbreviated pl still has some problems, especially for wavelength 355 nm. That lidar group will need to improve its algorithm. The mean relative errors of the French group for case 3 are ∼10%. However, all curves (including that of the French group) have similar values in the final stage [Figs. 3(a), 3(c), and 3(d) and 5(a), 5(c), and 5(d). In the range 3.0225–15.0675 km the mean absolute error for all groups is smaller than 1×10^{-5} (km sr)$^{-1}$.

The algorithm intercomparison shows that in general the data evaluation schemes of the different lidar groups work well. Differences in the solutions can be attributed mainly to differences in the estimation of input parameters. If the input parameters are known, the remaining mean relative errors are of the order of a few percent.

It should be stated also that, in case 3 situations, combined photometer–lidar observations would be useful. Our simulations indicate that even with a height-dependent lidar ratio the solution for the
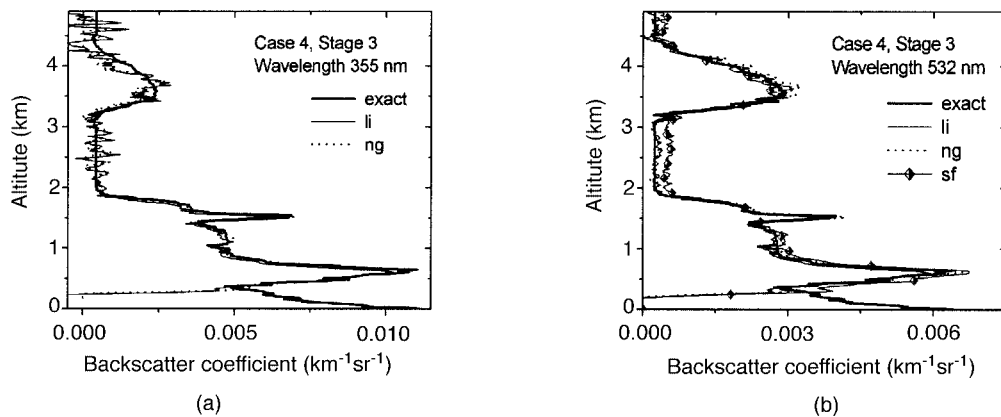
Fig. 6. Retrieved particle backscatter-coefficient profiles compared with the simulation input profiles for the wavelengths (a) 355 nm and (b) 532 nm for case 4 for the third stage. li, ng, and sf are abbreviations for three of the lidar system groups.

backscatter-coefficient profile calculated with the column lidar ratio as input is similar the solutions shown in Figs. 4 and 5.

The unknown reference value was of minor importance for the cases presented here, because height regions with dominating Rayleigh scattering were present in all cases. It should be mentioned, however, that such is not necessarily the case under realistic atmospheric conditions. Especially at 1064 nm, particle scattering often dominates the signals in the entire measurement range, which may cause additional errors that are not discussed here.

Case 4, the additional intercomparison, showed more-or-less the same qualitative behavior for stages 1, 2, and 3. In Fig. 6 the results of stage 3 for 355 and 532 nm show that the data evaluation schemes of the groups abbreviated li, ng, and sf work well, too. We remark that group be did not participate in case 4 because it uses exactly the same algorithm as group mi. Additionally, group li participated in case 4 because the development of its own algorithm was not finished for the major intercomparison.

In detail, the mean relative errors in stage 3 in the ranges 322.5–1987.5 m, i.e., in the lower layer, and 3217.5–3892.5 m, i.e., in the upper layer, are 11.35% ± 12.6% and 15.2% ± 10.6% for group li and 6.14% ± 8.9% and 26.8% ± 29.2% for group ng for wavelength 355 nm and are 7.35% ± 6.3% and 11.7% ± 16.2% for group li, 6.8% ± 6.7% and 10.8% ± 8.0% for group ng, and 14.51% ± 19.61% and 10.96% ± 12.3% for group sf for wavelength 532 nm. The mean relative errors show the same qualitative behavior as for case 3 with respect to wavelengths 355 and 532 nm. They are bigger for the smaller wavelength. Furthermore, the errors in general are smaller in the lower layer. In contrast to case 3, case 4 includes realistic signal noise. For this reason the values of the mean relative errors are bigger as for case 3 and, therefore, are not directly comparable.

Some additional remarks are in order. First, (1) groups at and th use only the wavelengths 355 and 532 nm at their lidar stations, (2) the lidar of group lk emits only at 355 nm, and (3) the lidar of group sf emits only at 532 nm. Therefore those groups did not perform evaluations at 1064, 532, and 355 nm, respectively. Second, groups na and po use a joint algorithm. Finally, groups mi and be deal with another joint algorithm.

5. Conclusions

An intercomparison of backscatter algorithms has been performed in three stages that represent increasing knowledge of the necessary input parameters. In stage 1 neither the necessary reference value nor the height-dependent lidar ratio was given. In stage 2 the prescribed lidar ratio was provided, and in stage 3 the reference value was also given. It became clear that the estimation of the lidar ratio that is required for real measurements has a large effect on the calculated aerosol backscatter profile. The calculated profiles can differ by more than 50% if no information on the lidar ratio is available. This effect decreases with increasing wavelength. Therefore additional measurements, such as sunphotometer observations, are of importance because they can provide the needed lidar-ratio information.

The effect of the reference value was rather small in the chosen cases; however, at 1064 nm the result can depend strongly on this value, which also has to be estimated for real measurements. The errors of the algorithms themselves, when all input parameters were known, were tested in stage 3. The remaining mean relative errors of the calculation in cases 2 and 3 are at the order of 2%–4% and can be regarded as negligible when they are compared to the uncertainties caused by misestimation of the input parameters' lidar ratio and reference value.

References

1. J. Bösenberg, A. Ansmann, J. M. Baldasano, D. Balis, C. Böckmann, B. Calpini, A. Chaikovsky, P. Flamant, A. Hågård, V. Mitev, A. Papayannis, J. Pelon, D. Resendes, J. Schneider, N. Spinelli, T. Trickl, G. Vaughan, G. Visconti, and M. Wiegner, "EARLINET: a European aerosol research lidar network," in *Advances in Laser Remote Sensing*, A. Dabas, C. Loth, and J. Pelon, eds., Selected papers of the 20th International Laser Radar Conference, Vichy, France (Ecole-Polytechnique, Palaiseau, France, 2000), pp. 155–158.

2. A. Ansmann, M. Riebsell, and C. Weitkamp, "Measurement of atmospheric aerosol extinction profiles with a Raman lidar," Opt. Lett. **15,** 746–748 (1990).

3. V. Matthias, J. Bösenberg, V. Freudenthaler, A. Amodeo, I. Balin, D. Balis, A. Chaykovski, G. Chourdakis, A. Comeron, A. Delaval, F. De Tomasi, R. Eixmann, A. Hågård, L. Komguem, S. Kreipl, R. Matthey, V. Rizi, J. A. Rodriguez, U. Wandinger, and X. Wang, "Aerosol lidar intercomparisons in the framework of the EARLINET project. 1. Instruments," Appl. Opt. **43,** 961–976 (2004).

4. J. Bösenberg, M. Alpers, D. Althausen, A. Ansmann, C. Böckmann, R. Eixmann, A. Franke, V. Freudenthaler, H. Giehl, H. Jäger, S. Kreipl, H. Linne, V. Matthias, I. Mattis, M. Müller, J. Sarközi, L. Schneidenbach, J. Schneider, T. Trickl, E. Vorobieva, U. Wandinger, and M. Wiegner, "The German aerosol lidar network: methodology, data, analysis," Rep. 317 (Max-Planck-Institut für Meteorologie, Hamburg, Germany, 2001).

5. S. Godin, A. I. Carswell, D. P. Donovan, H. Claude, W. Steinbrecht, I. S. Mcdermid, T. J. McGee, M. R. Gross, H. Nakane, D. P. J. Swart, H. B. Bergwerff, O. Uchino, P. von der Gathen, and R. Neuber, "Ozone differential absorption lidar algorithm intercomparison," Appl. Opt. **38,** 6225–6236 (1999).

6. W. Steinbrecht, H. Jäger, A. Adriani, G. di Donfrancesco, J. Barnes, G. Beyerle, R. Neuber, C. David, S. Godin, D. Donovan, A. I. Carswell, M. Gross, T. McGee, F. Masci, A. D'Altorio, V. Rizi, G. Visconti, I. S. McDermid, G. Megie, A. Mielke, B. Stein, C. Wedekind, T. Nagai, O. Uchino, H. Nakane, M. Osborn, and D. Winkler, "NDSC (Network for the Detection of Stratospheric Change) intercomparison of stratospheric aerosol processing algorithms," in *Advances in Atmospheric Remote Sensing with Lidar*, A. Ansmann, R. Neuber, P. Rairoux, and U. Wandinger, eds. (Springer-Verlag, Berlin, 1997), pp. 501–504.

7. C. Böckmann, U. Wandinger, A. Ansmann, J. Bösenberg, V. Amiridis, A. Boselli, A. Delaval, F. De Tomasi, M. Frioud, M. Iarlori, L. Komguem, S. Kreipl, G. Larchevêque, V. Matthias, A. Papayannis, F. Rocadenbosch, J. Schneider, V. Shcherbakov, and M. Wiegner, "EARLINET–backscatter lidar algorithm intercomparison," in *Proceedings of the 21st International Laser Radar Conference: Lidar Remote Sensing in Atmospheric and Earth Sciences*, L. R. Bissonnette, G. Roy, and G. Vallee, eds. (Defence R&D Canada, Valcartier, Quebec, Canada, 2002), pp. 353–356.

8. C. Böckmann, U. Wandinger, A. Ansmann, J. Bösenberg, V. Amiridis, A. Boselli, A. Delaval, F. De Tomasi, M. Frioud, M. Iarlori, L. Komguem, S. Kreipl, G. Larchevêque, V. Matthias, A. Papayannis, F. Rocadenbosch, J. Schneider, V. Shcherbakov, and M. Wiegner, "EARLINET—lidar algorithm intercomparison," J. Aerosol Sci. **32,** S433–S434 (2001).

9. A. Amodeo, G. Pappalardo, U. Wandinger, V. Matthias, J. Bösenberg, M. Alpers, F. De Tomasi, M. Frioud, M. Iarlori, L. Komguem, G. Larchevêque, A. Papayannis, and X. Wang, "Raman lidar algorithm intercomparison in the frame of EARLINET," in *Proceedings of the 21st International Laser Radar Conference: Lidar Remote Sensing in Atmospheric and Earth Sciences*, L. R. Bissonnette, G. Roy, and G. Vallee, eds. (Defence R&D Canada, Valcartier, Quebec, Canada 2002), pp. 349–352.

10. G. Pappalardo, A. Amodeo, M. Pandolfi, U. Wandinger, A. Ansmann, J. Bösenberg, V. Matthias, V. Amiridis, F. De Tomasi, M. Frioud, M. Iarlori, L. Komguem, A. Papayannis, F. Rocadenbosch, and X. Wang, "Aerosol lidar intercomparisons in the framework of EARLINET. 3. Raman lidar algorithm for aerosol extinction, backscatter, and lidar ratio," Appl. Opt., submitted for publication.

11. J. D. Klett, "Stable analytical inversion solution for processing lidar returns," Appl. Opt. **20,** 211–220 (1981).

12. J. D. Klett, "Lidar inversion with variable backscatter/extinction ratios," Appl. Opt. **24,** 1638–1643 (1985).

13. F. G. Fernald, B. M. Herman, and J. A. Reagan, "Determination of aerosol height distributions by lidar," J. Appl. Meteorol. **11,** 482–489 (1972).

14. F. G. Fernald, "Analysis of atmospheric lidar observations: some comments," Appl. Opt. **23,** 652–653 (1984).

15. A. Bucholtz, "Rayleigh-scattering calculations for the terrestrial atmosphere," Appl. Opt. **34,** 2765–2773 (1995).

16. E. J. McCartney, *Optics of the Atmosphere, Scattering by Molecules and Particles* (Wiley, New York, 1976).

17. B. A. Bodhaine, N. Wood, E. Dutton, and J. Slusser, "On Rayleigh optical depth calculations," J. Atmos. Ocean. Technol. **16,** 1854–1861 (1999).

18. Y. Sasano, E. V. Browell, and S. Ismail, "Error caused by using a constant extinction/backscattering ratio in the lidar solution," Appl. Opt. **24,** 3929–3932 (1985).

19. V. A. Kovalev and H. Moosmüller, "Distortion of particulate extinction profiles measured with lidar in a two-component atmosphere," Appl. Opt. **33,** 6499–6507 (1994).

20. M. Matsumoto and N. Takeuchi, "Effects of misestimated far-end boundary values on two common lidar inversion solutions," Appl. Opt. **33,** 6451–6456 (1994).

21. J. Bösenberg, R. Timm, and V. Wulfmeyer, "Study on retrieval algorithms for a backscatter lidar," Rep. 226 (Max-Planck-Institut für Meteorologie, Hamburg, Germany, 1997).

22. U.S. Committee on Extension to the Standard Atmosphere, *U.S. Standard Atmosphere* (National Oceanic and Atmospheric Administration, Washington, D.C., 1976).

23. U. Wandinger and A. Ansmann, "Experimental determination of the lidar overlap profile with Raman lidar," Appl. Opt. **41,** 511–514 (2002).